Secondary eyewall formation as a progressive boundary layer response

S. F. Abarca[1], M. T. Montgomery[1] and M. M. Bell[2]

[1]Naval Postgraduate School, Monterey, CA [2]University of Hawaii, Honolulu, HI

Secondary eyewall essentials

Secondary eyewalls (SEs) are structures concentric to the storm's primary eyewall, characterized by maxima in the azimuthally averaged convective activity and tangential winds. It is well know that SEs are related to storm intensity change and storm growth and there is robust observational evidence, based on satellite surveillance (e.g. Fig. 1), that secondary eyewalls are common features in major hurricanes. Such a robust remote monitoring contrast with the **scarce *insitu* observations** of the phenomena life cycle. The latter has limited the SE formation (SEF) understanding.

A wide variety of physical processes have been invoked to explain SEF, but only the recently proposed theory of a **progressive boundary layer control** in SEF has been supported by a variety of full physics mesoscale numerical integrations (Huang et al. 2012; Abarca et al. 2012).

We present here a new approach to test the newly proposed SEF theory. We integrate a simple axisymmetric slab boundary layer model to see whether such a reduced numerical framework generates SEs when initialized and forced with those vortex structures of a real and a numerical storm (see below) that undergo SEF. i.e. **we test whether boundary layer dynamics, in isolation from moist dynamics and the presence of asymmetries and their effects, can result in SEF.**

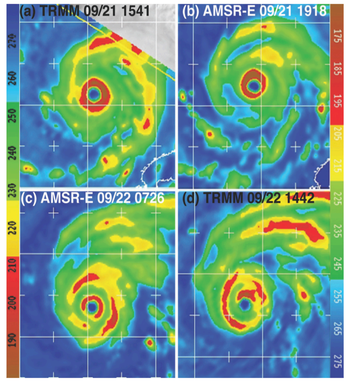

Fig. 1. Hurricane Rita (2005) brightness temperatures from (a),(d) TRMM/TMI (at 85 GHz) and (b),(c) Aqua/AMSR-E (at 89 GHz) polar- orbiting microwave satellites at four times. Color scales on left and right correspond to TRMM and AMSR-E temperatures, respectively. White tick marks are every 18 with solid white lines every 28 of latitude and longitude. Taken from Bell et al. (2012).

Field campaign and realistic numerical simulation data

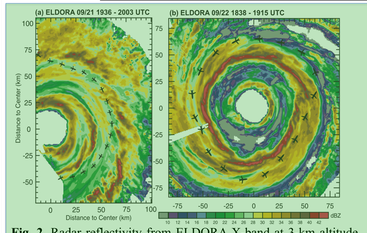

Fig. 2. Radar reflectivity from ELDORA X-band at 3-km altitude during (a) 1936–2003 UTC 21 September and (b) 1838–1915 UTC 22 September. Taken from Bell et al. (2012).

- Hurricane Rainband and Intensity Change Experiment (**RAINEX**) field campaign
- Multiplatform observations of Hurricane Rita (2005) during secondary eyewall stage (21-22 September)
  - Satellite (Fig. 1)
  - Doppler radar (Fig. 2)
  - Aircraft (Fig. 3)
- Limited data during the emergence of tangential wind secondary maximum (Fig. 3)

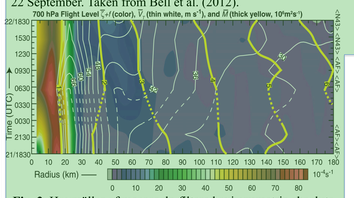

Fig. 3. Hovmöller of mesoscale-filtered axisymmetric absolute vertical vorticity (color, 1024 s21) and tangential wind (contour, m s21) at 700-hPa flight level from 1830 UTC 21 Sep to 1830 UTC 22 Sep. Aircraft passes corresponding to analysis times are shown on the right ordinate. Dashed contours indicate linearly interpolated data between aircraft missions.

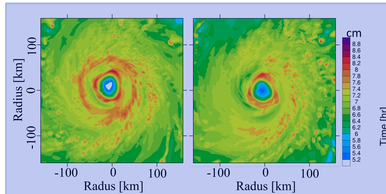

Fig. 4. WRF Rita simulation precipitable water (cm) snapshots for during a) 21:00 UTC 21 September and b) 07:00 UTC 22 September

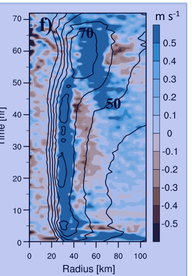

Fig. 5. WRF Rita simulation Hovmöller diagram of azimuthally averaged 850 hPa tangential wind magnitude [m s^{-1}, colors] and vertical velocity [m s^{-1}, shaded), taken from Abarca and Corbosiero (2011).

- WRF model, deemed the Advanced Hurricane WRF (Davis et al., 2008)
- Three domains (12, 4 and 1.33 km) with two-way movable nests
- Kain-Fritsch cumulus parameterization (only in the outer domain)
- WRF single-moment 5-class microphysics scheme
- Yonsei University scheme for the planetary boundary layer (Noh et al. 2003)
- The surface drag algorithm follows Charnock (1955)
- Surface exchange coefficient for heat flux (Skamarock et al. 2005) and for water vapor (Carlson and Boland 1978)

Slab boundary layer dynamics generate secondary wind maxima in response to observed hurricane radial structures

Slab boundary Layer model (Slab-BL)

- Slab boundary layer model (based on Shapiro 1983)
- Integrates the equations:

$$\frac{\partial\langle u\rangle}{\partial t}=-\langle u\rangle\frac{\partial\langle u\rangle}{\partial r}+\frac{\langle v\rangle^2}{r}+f\langle v\rangle-\frac{C_D}{h}\langle u\rangle\left(\langle u\rangle^2+\langle v\rangle^2\right)^{1/2}-K\left(\nabla^2\langle u\rangle-\frac{\langle u\rangle}{r^2}\right)-\frac{1}{\rho}\frac{\partial\langle p\rangle}{\partial r} \quad (1)$$

$$\frac{\partial\langle v\rangle}{\partial t}=-\langle u\rangle\frac{\partial\langle v\rangle}{\partial r}-\langle u\rangle\frac{\langle v\rangle}{r}-f\langle u\rangle-\frac{C_D}{h}\langle v\rangle\left(\langle u\rangle^2+\langle v\rangle^2\right)^{1/2}-K\left(\nabla^2\langle v\rangle-\frac{\langle v\rangle}{r^2}\right) \quad (2)$$

- **Model parameters**
  - Boundary layer depth
    h=1.5 km
  - Drag coefficient (Thomsen et al. 2012)
    $C_D=0.7\times10^{-3}+1.4\times10^{-3}(1-\exp(-0.055<u>^2+<v>^2)0.5)$
  - Eddy diffusivity
    K=1 × 10^4 m^2 s^{-1}

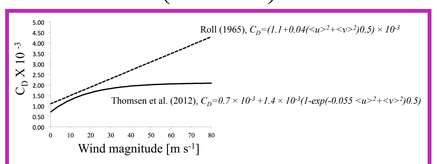

Sensitivity experiments to the 3 model parameters render results consistent with those presented here

- Initialized and forced (through the radial pressure gradient term in Eq. (1)) with RAINEX and AHW data.

Slab-BL and RAINEX, 49 integrations

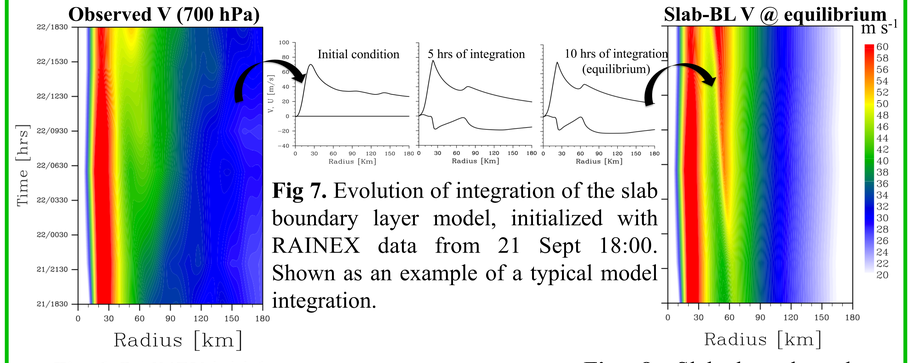

Fig 7. Evolution of integration of the slab boundary layer model, initialized with RAINEX data from 21 Sept 18:00. Shown as an example of a typical model integration.

Fig. 6. RAINEX initial conditions & forcing (as Fig. 3)

Fig. 8. Slab boundary layer model integration at equilibrium.

- **All 49** integrations render an equilibrium state (reached at about hour 11 of integration) with a **SE pattern**.
- Time evolution of the integrations ubiquitously show **contracting SEs**.
- The slab boundary layer SEs are **qualitatively comparable** to the observed one (radial location, tangential and radial wind magnitude)

Slab-BL and AHW, 73 integrations

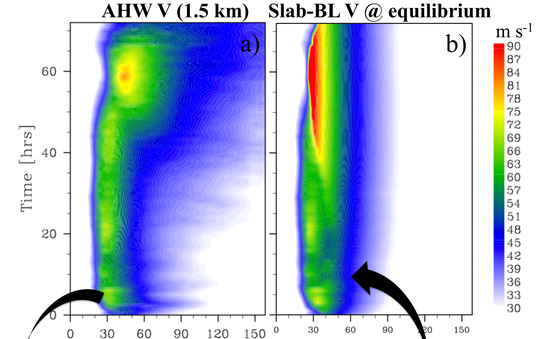

Fig. 9. As Fig. 6 but using AHW model data at 1,500 m instead of the 700 hPa from RAINEX.

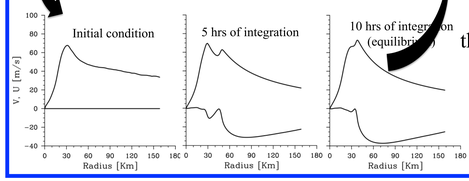

Fig. 10. Evolution of integration of the slab boundary layer model, initialized with hour 40 AHW integration data.

Conclusions

Slab boundary layer dynamics undergo SEF when forced with radial structures of hurricanes (observed and synthetic) that also undergo SEF. Slab-BL SEF occurs without other hurricane dynamical elements (e.g. vortex asymmetries, moist dynamics, WISHE feedback, neighboring eddies).

Slab boundary layer SEs are in qualitative agreement with those in nature and in realistic model integrations. They also exhibit behavior as SE radial contraction, eyewall replacement cycle and eyewall merger. This suggests that boundary layer dynamics may be playing an unforeseen role in eyewall replacement cycles.

Acknowledgements

The first author gratefully acknowledges the support from the National Research Council (NRC), through its Research Associateship Program, and the host institution, the Naval Postgraduate School (NPS) in Monterey, California. The work was partially supported by the Office of Naval Research (ONR), through award N0001411WX20095, and by the National Science Foundation (NSF), through award AGS 0733380.

References

Abarca, S. F., and M. T. Montgomery, 2012: Essential dynamics of secondary eyewall formation. , *J. Atmos. Sci. Submitted*.

Abarca, S. F., and K. L. Corbosiero, 2011: Secondary eyewall formation in WRF simulations of hurricanes Rita and Katrina (2005). Geophys. Res. Lett., 38, L07802.

Bell, M. M., M. T. Montogmoer and W. C. Lee, 2012: An axisymmetric view of concentric eyewall evolution in Hurricane Rita (2005), *J. Atmos. Sci., 69: 2414-2432*.

Charnock, H., 1955: Wind stress on a water surface. *Quart. J. Roy. Meteor. Soc.*, **81.**

Carlson, T. N., and F. E. Boland, 1978: Analysis of urban-rural canopy using a surface heat flux/temperature model. *J. Appl. Meteor.*, **17,** 998–1013.

Davis, C., W. Wang, S. S. Chen, Y. Chen, K. L. Corbosiero, M. DeMaria, J. Dudhia, G. Holland, J. Klemp, J. Michalakes, H. Reeves, R. Rotunno, C. Snyder and Q. Xiao, 2008: Prediction of landfalling hurricanes with the Advanced Hurricane WRF Model. *Mon. Wea. Rev.*, **136**, 1990–2005.

Huang, Y. H., M. T. Montgomery and C. C. Wu, 2012: Concentric eyewall formation in typhoon Sinlaku (2008). Part II: Axisymmetric Dynamical Processes. *J. Atmos. Sci.* **69:** 662-674. **687.**

Noh, Y., W. G. Cheon, S. Y. Hong, and S. Raasch, 2003: Improvement of the K-profile model for the planetary boundary layer based on large eddy simulation data. *Bound. Layer Meteor.*, **107,** 421–427.

Skamarock, W. C., J. B. Klemp, J. Dudhia, D. O. Gill, D. M. Barker, W. Wang, and J. G. Powers, 2005: A description of the Advanced Research WRF version 2, NCAR Tech. Note TN-468+STR, 88 pp.

Shapiro, L. J., 1983: The Asymmetric Boundary layer Flow Under a Translating Hurricane. *J. Atmos. Sci.*, **40,** 1984–1998.

Roll, H. U., 1965: *Physics of the Marine Atmosphere.* International Geophysical Series, Vol. 7, Academic Press, 426 pp.

Thomsen, G., M. T. Montgomery and R. Smith, 2012: Sensitivity of tropical cyclone intensification to perturbations in the surface drag coefficient, *Q. J. R. Meteorol. Soc., in press*.